

Article

Symmetric Nonlinear Feedback Control and Machine Learning for Sustainable Spherical Motor Operation

Marwa Hassan ¹, Eman Beshr ¹, Mahmoud Beshr ¹ and Ali M. El-Rifaie ^{2,*} 

¹ Arab Academy For Science and Technology and Maritime Transport, Sheraton Al Matar, P.O.2033 Elhorria, Cairo 11311, Egypt; eng_marwa@aast.edu (M.H.); beshre@aast.edu (E.B.); mbeshr@aast.edu (M.B.)

² College of Engineering and Technology, American University of the Middle East, Egaila 54200, Kuwait

* Correspondence: ali.el-rifaie@aum.edu.kw

Abstract: This paper presents a comprehensive evaluation of a new control technique for the sphere motor system, aimed at achieving accurate tracking, robust and dispersion of vibrations. Control methods include the determination of a nonlinear model and the application of feedback linearization, followed by the optimization of the proportional derivative (PD) coefficients through the Adaptive Neuro-Fuzzy Inference System. In addition, the system's reaction to harsh environments is managed using Long Short-Term Memory. In order to gain a deeper understanding, symmetrical environmental disturbances and trajectories are introduced during the testing phase. The results demonstrate the superior performance of the control strategy, with reduced vibrations, faster recovery and confirmed tracking accuracy. In addition, the control method shows its adaptability and reliability, as evidenced by the significant reduction in CO₂ emissions compared to conventional PD control methods. The use of symmetric trajectories and visualizations further emphasizes the behavior of the system under symmetric conditions, strengthening the effectiveness and applicability of the control strategy in real-world scenarios. Overall, this study presents a promising solution for converting complex systems under different conditions and making them potentially applicable in various industrial contexts.

Keywords: feedback linearization; symmetric disturbances; symmetric trajectories; spherical motors; Adaptive Neuro-Fuzzy Inference System; artificial intelligence; PD controller; carbon dioxide emission; nonlinear systems; environmental impact



Citation: Hassan, M.; Beshr, E.; Beshr, M.; El-Rifaie, A.M. Symmetric Nonlinear Feedback Control and Machine Learning for Sustainable Spherical Motor Operation. *Symmetry* **2023**, *15*, 1661. <https://doi.org/10.3390/sym15091661>

Academic Editors: Quanxin Zhu, Zuwei Cai and Fanchao Kong

Received: 30 July 2023

Revised: 18 August 2023

Accepted: 23 August 2023

Published: 28 August 2023



Copyright: © 2023 by the authors. Licensee MDPI, Basel, Switzerland. This article is an open access article distributed under the terms and conditions of the Creative Commons Attribution (CC BY) license (<https://creativecommons.org/licenses/by/4.0/>).

1. Introduction

Multiple-degree actuators are important components that are widely used in different industries and serve a wide range of applications, from robotic weapons to aerospace systems. Traditional actuators are usually used to connect pairs of a single degree of freedom motors using series or parallel configuration gears and connections [1–4]. However, these conventional actuators have several limitations, such as large size, high mass, a reduced positioning accuracy and workspace specificity. As the industry demands more accurate trajectory planning and regulation capabilities, innovative multi-degree freedom actuator systems have become essential. In response to the limitations of conventional actuators, sphere motors (SMs) have emerged as promising solutions. These multi-DOF actuators have numerous advantages, including a compact and light design, an increased positioning accuracy, mechanical deformation, friction and backlash reduction [5–8]. As a result, SMs have been found to be suitable for various applications that require the accurate and continuous control of multiple degrees of movement, covering areas such as robotics, aerospace and medical devices [9–17].

Despite their advantages, SMs also pose certain challenges and need to be carefully considered in the design of control systems. One of the main obstacles to the effective control of sphere motors is their inherent nonlinearity, which results from the complex

interaction between the motor and the gimbal mechanism. This nonlinearity can lead to unpredictable behavior, making accurate trajectory planning and regulation more difficult. Addressing this nonlinearity is essential to achieve a strong and accurate control of the SM. Furthermore, significant energy consumption from SMs contributes to carbon dioxide emissions and contributes to climate change. As a result, environmental concerns have increased, and it is urgent to adopt a sustainable energy-efficient control strategy to minimize the carbon footprint of spherical motors.

In addition, the adverse effects of environmental condition changes caused by changes in the climate could lead to a reduction in the lifespan of spherical engines, emphasizing the need for sustainable solutions to extend their operational life and reduce the overall impact on the environment. The review of the literature on the control system technology of spherical engines revealed significant advances and applications aimed at overcoming their challenges. Feedback control theory has evolved since the development of the post-World War II period, and has become widely adopted in the process industry [18–21]. Nicholas Minorsky's 1922 groundbreaking work on three-term or PID controllers and James Watt's introduction of the 16th century Centrifugal Governor laid the foundations for modern feedback control techniques [22]. There are various control schemes for sphere engines, with joint and operational space control being prominent approaches, each addressing specific mechanical design aspects [23–31]. Joint space control focuses on the design of feedback controllers that closely align the actual movement and the desired movement, typically converting the desired movement into a joint variable and controlling each joint independently. Operational space control, on the other hand, aims to create a feedback controller that allows the actual motion of the end effector to follow the desired motion of the end effector, which often requires more complex algorithms and reverse motion [32–34]. In order to address the nonlinearity of SMs and achieve acceptable performance for uncertain systems, researchers have used various nonlinear control methods. This includes feedback linearization, which transforms nonlinear dynamics into a linear form and facilitates the application of classical control techniques. Passivity control, sliding mode control, artificial intelligence control, Lyapunov control and adaptive control are other approaches to improve stability and control accuracy through understanding the nonlinearity of system dynamics [35–39].

However, these nonlinear control strategies may still face challenges related to robustness, convergence and the complexity of real-world systems.

The integration of AI techniques with traditional controllers, such as fuzzy logic and neural networks, has shown promise in achieving robust and accurate control for spherical motors [39]. The combination of fuzzy logic and neural networks in an Adaptive Neuro-Fuzzy Inference System (ANFIS) provides a powerful tool to handle nonlinearity and uncertainty in complex systems. Despite the application of AI-based control techniques for spherical motors, challenges remain due to the inherent complexities and nonlinearities. While AI shows promise, it may encounter limitations in certain scenarios, potentially leading to less-than-optimal results. As the field of spherical motor control advances, researchers strive to refine AI-driven strategies to overcome these obstacles, aiming for an improved control of the multi-degree-of-freedom capabilities of spherical motors [40–51].

Another potent tool in controlling complex systems, including power systems, is the Long Short-Term Memory (LSTM) algorithm [52–55]. LSTM's ability to handle time-series data and predict future behavior based on past observations has made it valuable for various applications. In the context of spherical motors, LSTM can be utilized to predict the SM's response under varying environmental conditions, enabling the control system to adjust proactively and improve its robustness.

In the context of controlling spherical motors, the concept of symmetry plays a crucial role in enhancing system performance and stability. By introducing symmetric disturbances and trajectories during testing, researchers can gain valuable insights into how the control strategy responds to symmetric challenges. This is particularly important as real-world ap-

plications often involve disturbances and environmental conditions that exhibit symmetric characteristics [56–59].

Designing task frame trajectories to exhibit symmetry with respect to corresponding joints further reinforces the control approach's effectiveness. Symmetric trajectories enable the control system to handle the complex interaction between the motor and gimbal mechanism more effectively, leading to improved trajectory tracking and regulation capabilities. The use of symmetric trajectories also helps in reducing unpredictable behaviors arising from system nonlinearity, resulting in more accurate and robust control.

By emphasizing the symmetric aspects through visualizations and graphs, such as overlaid plots for symmetric joints and task frame trajectories, we can better understand the system's behavior under symmetric conditions. This approach allows us to identify any potential issues related to symmetry and provides an opportunity to fine-tune the control strategy for optimal performance in such scenarios.

Driven by the imperative to address the innate complexities and uncertainties inherent to spherical motors (SMs), which often hinder precise trajectory planning, stability and control, this paper introduces a sophisticated control paradigm poised to enhance their performance. The integration of feedback linearization and ANFIS offers a comprehensive strategy to navigate the intricate dynamics of SMs, enabling more accurate trajectory tracking and stability. With the additional integration of LSTM, the approach gains predictive prowess, fortifying its robustness under challenging environmental conditions and paving the way for more adaptable and dependable control strategies. The study's emphasis on symmetry in testing and trajectory design further underscores its comprehensive approach to bolster control effectiveness. This research thus propels spherical motor control toward more accurate, dependable and sustainable applications across various industries. As the horizon of possibilities beckons, future work may involve practical hardware testing to validate the approach's real-world reliability, accounting for complexities beyond the current dynamical model.

This paper is organized as follows: Section 1 introduces the importance of the SM and its history. Section 2 provides an in-depth exploration of the spherical motor's integrated modeling and control strategy. This comprehensive section encompasses the modeling of the SM as well as the detailed presentation of the proposed control strategy, which includes aspects like nonlinear feedback design, ANFIS and LSTM data systems. Notably, this section also addresses the mathematical proofs for the stability of the control system. Through a rigorous application of Lyapunov's Direct Method, the stability of the closed-loop control system is rigorously established. By leveraging Lyapunov Stability Analysis, the proposed control technique's stability is substantiated, providing a robust mathematical foundation for the efficacy and reliability of the control strategy in ensuring the stable operation of the spherical motor (SM) system.

Section 3 illustrates the proposed controller, simulations and results. Finally, Section 4 presents the conclusion, summarizing the key findings of the study.

2. Modeling and Control

This section delves into the comprehensive analysis of the system's model and the implementation of advanced control strategies, namely Nonlinear Feedback (NLF), Adaptive Neuro-Fuzzy Inference System (ANFIS) and Long Short-Term Memory (LSTM). Each technique's design principles are discussed individually.

2.1. Modeling

The linear and nonlinear behavior of the spherical motor (SM) can be illustrated through the study of the dynamical modeling. In this model, the relation starts from motion, torque, acceleration, velocity and force until the current and voltage are described. Moreover, particularly dynamic effects such as inertia and centrifugal are also described in it [26]. As for the nonlinear and the uncertain dynamics' parameters, they have three degrees of freedom. The structure of SM is shown in Figure 1.

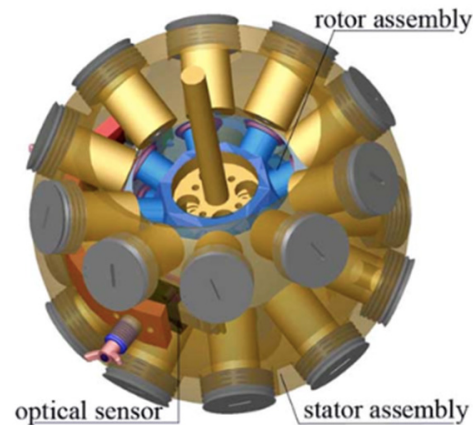


Figure 1. Mechanical structure of SM [25].

The SM is governed by the following equation:

$$F(q) \begin{bmatrix} \ddot{\alpha} \\ \ddot{T} \\ \ddot{\gamma} \end{bmatrix} + T(q) \begin{bmatrix} \dot{\alpha}\dot{T} \\ \dot{\alpha}\dot{\gamma} \\ \dot{T}\dot{\gamma} \end{bmatrix} + R(q) \begin{bmatrix} \dot{\alpha}^2 \\ \dot{T}^2 \\ \dot{\gamma}^2 \end{bmatrix} = \begin{bmatrix} \tau_x \\ \tau_y \\ \tau_z \end{bmatrix} \quad (1)$$

where $F(q)$ represents a positive and geometric inertia matrix, $T(q)$ is the Coriolis torques, $R(q)$ is the centrifugal torque matrix, and finally, τ is the actuation torque of x , y and z directions. It can be noted from the above equation that the angular acceleration is influenced by a double integrator; therefore, it can be considered a decoupled system with a second-order equation. As a result of the decoupling effect, all parameters will depend on each other except for the motion variable q_i ; hence, the acceleration \ddot{q} can be rewritten as:

$$\ddot{q} = F^{-1}(q) (\tau_x + \tau_y + \tau_z + \tau \dot{d}) + R(q) \quad (2)$$

When referring to the study of the spherical motor, two main parts must be considered. First, the kinematics effect, which is the calculation of the rigid bodies and the final part, without taking into account the effect of any calculated forces. Secondly, the study of the dynamics depends on the design of the controller and its behavior in the actual situation.

Based on [21], the kinematics is divided into two main parts: inverse and forward. Inverse kinematics is used to determine all possible joints' variables when all positions and orientations of the task frame can be active. Forward kinematics is used to determine all the positions and orientations of the task frame when the joint position is known. The main purpose of Forward Kinematics (FK) is to calculate:

$$\gamma(x, q) = 0 \quad (3)$$

γ represents a nonlinear function while $x = [x_1 \cdots x_n]$ is the variable task space. Usually, there are three orientations and three task spaces. The vector displacement is represented by the $[q_1 \cdots q_L]^T$ vector, where L is the number of joints.

To calculate the FK, the Denavit–Hartenberg convention is used. The primary step is to determine the DH parameter through the following standard steps: (a) the allocation of the motor; (b) the joint labeling; (c) the joint rotation determination; (d) the base setup for the coordinate frame; (e) the joint coordination setup; (f) the determination of the link twist; (g) the determination of C_i and G_j , where C_i is the link length offset while G_j is the distance between X_{i-1} and X_i along the z axis; and (h) concluding the DH Table. The final stage is to compute the relation matrix Rn^* starting from G_j to G_{j-1} , using the following formula:

$$R_j^{j-1} = U_j(\alpha_j) N_j(\theta_j) \quad (4)$$

where

$$U_j(\theta_j) = \begin{bmatrix} \cos(\alpha_j) & -\sin(\alpha_j) & 0 \\ \sin(\alpha_j) & \cos(\alpha_j) & 0 \\ 0 & 0 & 1 \end{bmatrix} \quad (5)$$

$$N_j(\theta_j) = \begin{bmatrix} 1 & 0 & 0 \\ 0 & \cos(\theta_j) & -\sin(\theta_j) \\ 0 & \sin(\theta_j) & \cos(\theta_j) \end{bmatrix}$$

and so, R^0_j is given by:

$$R^0_j = [(U_1 N_1) \cdots (U_n N_n)] \quad (6)$$

Finally, the transformation matrix is calculated through:

$$P^0_j = P^0_1 P^1_2 \cdots P^{j-1}_j = \begin{bmatrix} R^0_j & 0 \\ 0 & 1 \end{bmatrix} \quad (7)$$

2.2. Control Strategy

This section is divided by subheadings. It should provide a concise and precise description of the experimental results, their interpretation, as well as the experimental conclusions that can be drawn.

2.2.1. NLFC

One of the main issues that face the control of the spherical motor is the uncertainty of the dynamics. Feedback Linearization is a very well-known technique that can be used to overcome this; in addition, it can be used to overcome stability and disturbance issues. The main concept is to design feedback that can track a certain behavior, which, in this case, is the desired manipulator motion q_g :

$$e^*(t) = q_g(t) - q_h(t) \quad (8)$$

where $q_g(t)$ and $q_h(t)$ refer to the desired and the actual displacements, respectively, while $e(t)$ refers to the error. The state-space equation of the linearized model can be:

$$\dot{x} = Gx + Bu \quad (9)$$

$$G = \begin{bmatrix} 0 & I \\ 0 & 0 \end{bmatrix}, B = \begin{bmatrix} 0 \\ 1 \end{bmatrix} \quad (10)$$

Using Brunovsky canonical form feedback,

$$U = -F^{-1}(q)N(q, \dot{q}) + H^{-1}\tau \quad (11)$$

can be defined and the Brunosky form can be rewritten as a function of the error and its derivative as:

$$\begin{bmatrix} \dot{e}^*(t) \\ e^*(t) \end{bmatrix} = \begin{bmatrix} 0 & I \\ 0 & 0 \end{bmatrix} \begin{bmatrix} \dot{e}^*(t) \\ e^*(t) \end{bmatrix} + \begin{bmatrix} 0 \\ 1 \end{bmatrix} u \quad (12)$$

with

$$u = q_g + F^{-1}N(q) \approx q_h \quad (13)$$

Then, the required arm torques can be calculated using the inverse of the previous equation:

$$\tau = F(q)(q_g - U) + N(q, \dot{q}) \quad (14)$$

The selected Nonlinear Feedback guarantees the tracking of the desired $q_g(t)$ trajectory. Finally, by adding the proportional with the derivative, the PD control in the form of $U = K_v \dot{e} + K_p e$ is selected, such that the torque is written as:

$$\tau = F(q)(q_g + K_v \dot{e} + K_p e) + N(q, \dot{q}) \tag{15}$$

where $N(q, \dot{q})$ is a nonlinear term of a system dynamics:

$$N(q, \dot{q}) = Zq[\dot{q}\dot{q}] + Mq[\dot{q}\dot{q}] \tag{16}$$

Applying PD control ensures that the error will converge to zero. The nonlinear torque controller is then summarized.

2.2.2. Adaptive Neuro-Fuzzy System (ANFIS)

Neuro-Fuzzy System has become a very important tool in recent years, especially in industrial applications whose processes are too complicated to be solved using classical approaches. It poses several advantages as it combines the benefits of the Artificial Neural Network (ANN) and Fuzzy Interference System (FIS) simultaneously.

Moreover, it overcomes the time-consuming process that is needed to tune the parameters of the fuzzy system and build the neural network structure. Adaptive Neuro-Fuzzy Interference System is one of the prominent methods that have been introduced by Jyh-Shing Roger in 1993 (Figure 2). It is considered a very powerful tool that processes a lot of advantages as it (1) can be easily used to model difficult functions; (2) enables fast and accurate learning; (3) can be imposed on many applications; and (4) can alter to unknown conditions. Till now, there are still developments in Neuro-Fuzzy synergisms for the adaptive control and modeling of nonlinear systems.

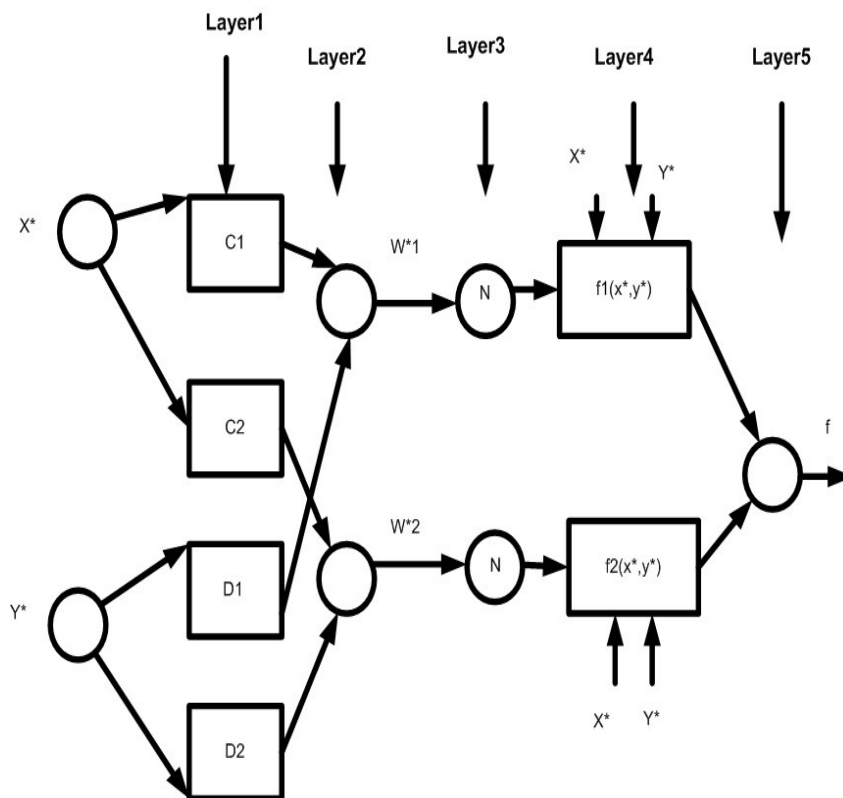


Figure 2. ANFIS structure.

Despite all the advantages mentioned before, there are still some deficiencies that are still under development in Neuro-Fuzzy synergisms for the adaptive control and modeling of nonlinear systems. Fuzzy logic is used to transform given inputs into desired output through highly interconnected neural network processing elements and information connection. The membership function must have the same number as the rule. A Fuzzy

Interference System (FIS) is constructed using training data. A hybrid system that consists of backpropagation and recursive least-square algorithms is used to adjust the FIS function parameters. In order to speed up the process, the hybrid techniques are introduced instead of the gradient method alone as it can be trapped in local minima. The FIS under consideration consists of two input values (x^* , y^*) and one output z^* . The base rule contains two “IF then” (Takagi and Sugenos) types:

$$\text{Rule 1 If } x^* \text{ is } C_1 \text{ and } y^* \text{ is } D_1. \text{ Then } f_1 = p_1x^* + q_1y^* + R_1 \quad (17)$$

$$\text{Rule 2 If } x^* \text{ is } C_2 \text{ and } y^* \text{ is } D_2. \text{ Then } f_2 = p_2x^* + q_2y^* + R_2 \quad (18)$$

In the next paragraph, the construction of the layer is illustrated as shown in Figure 2. First layer: In this layer, each node J is a square node with function

$$O_j^* = M_{C_j}(X^*) \quad (19)$$

where C represents the linguistic label associated with this node function, while x^* is the input to node j .

Second layer: Each node is a circle node labeled π and it multiplies the incoming signal and the outgoing products:

$$W_j^* = M_{C_j}(X^*) * M_{D_j}(X^*) \quad (20)$$

The output identifies the firing strength. The third layer is similar to the previous one, where the node is represented by a circle and the j th node is represented as:

$$w_j^{-*} = \frac{w_j^*}{w_1^* + w_2^*} \quad (21)$$

Fourth layer: Each node J is a square node, represented as:

$$O^4 = w^* f_j = W^{-*}(P_j X^* + Q_j Y^* + r_j) \quad (22)$$

Final layer: It consists of a single layer that is used to count the overall output:

$$o_j^* = \partial w^* \frac{\partial w_i}{\partial_i w_i} f_j \quad (23)$$

2.2.3. Long Short-Term Memory (LSTM)

Long Short-Term Memory (LSTM) is a powerful type of recurrent neural network (RNN) introduced by Hochreiter and Schmidhuber in 1997 [60]. Its primary purpose is to address the vanishing gradient problem frequently encountered in traditional RNNs, which hinders their ability to capture long-term dependencies in sequential data. LSTM's remarkable advantage lies in its capability to effectively handle long-term dependencies, making it a valuable tool for predicting sequences with intricate patterns over extended periods. Furthermore, LSTMs are well-suited for learning from large datasets, making them ideal for applications that require processing vast amounts of data. However, it is essential to note that LSTM models can be computationally expensive and may require a substantial amount of training data to achieve high accuracy.

In the context of the spherical motor, LSTM plays a crucial role in predicting the motor's response under harsh environmental conditions, such as varying temperature and humidity levels. To achieve this, historical data obtained by simulating the motor under different environmental scenarios, including the introduction of random noise, sudden changes in load or temperature and external disturbances, are used to train the LSTM model.

The LSTM model's cell-state update and hidden-state update equations are as follows:

$$C_t = f_t \cdot C_{t-1} + i_t \cdot C_t^* \quad (24)$$

$$h_t = o_t \cdot \tanh(C_t) \quad (25)$$

where C_t represents the cell state at time step t , f_t is the forget gate output at time step, i_t is the input gate, h_t is the hidden gate, while o_t is the output gate at time step. C_t^* refers to the candidate cell state (new information) at time step and \tanh is the hyperbolic tangent function.

To evaluate the robustness of the LSTM model, appropriate evaluation metrics, including Mean Squared Error (MSE), Root-Mean-Squared Error (RMSE) and Mean Absolute Error (MAE), are defined. These metrics provide a quantitative measure of the discrepancies between the model's predicted outputs and the actual responses of the system, allowing us to assess the accuracy and reliability of the LSTM model when faced with uncertainties and disturbances. The details of the operation are shown in Figure 3.

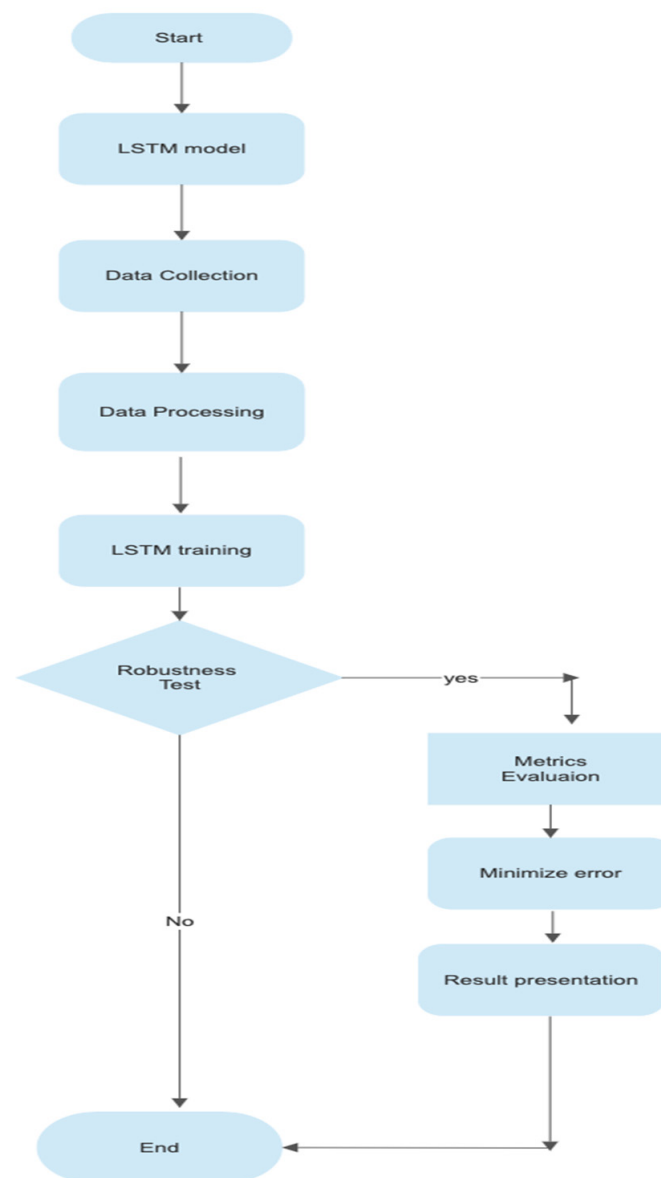


Figure 3. Detailed flow chart.

2.2.4. Lyapunov Stability Analysis

In the context of the proposed control technique for the spherical motor (SM) system, we will rigorously establish the stability using Lyapunov's Direct Method. This mathematical approach provides a robust proof of the system's stability under the proposed control strategy. Consider the closed-loop control system with the proposed controller as follows:

$$u(t) = K_{LSTM} \cdot (X_{ref}(t) - X(t)) \quad (26)$$

The K_{LSTM} represents the gain of the proposed controller, $X_{ref}(t)$ denotes the reference state and $X(t)$ signifies the current state of the system.

Theorem 1 (Lyapunov Stability). *If there exists a positive definite function $V(x)$, such that its derivative along the system trajectories is negative semi-definite, i.e., $V'(x) \leq 0$, then the closed-loop control system is stable.*

Proof. Let us choose a positive definite Lyapunov function candidate:

$$V(x) = (X_{ref}(t) - X(t))^T P (X_{ref}(t) - X(t)) \quad (27)$$

where P is a positive definite matrix. The time derivative of $V(x)$ along the system trajectories is given by:

$$V'(x) = -2 (X_{ref}(t) - X(t))^T P A (X_{ref}(t) - X(t)) \quad (28)$$

A is the system matrix.

For stability analysis, we require $V'(x) \leq 0$, which leads to the condition:

$$(X_{ref}(t) - X(t))^T P A (X_{ref}(t) - X(t)) \geq 0 \quad (29)$$

This simplifies to:

$$-2 (X_{ref}(t) - X(t))^T P A (X_{ref}(t) - X(t)) \leq 0$$

Dividing both sides by $(X_{ref}(t) - X(t))^T P$ and $X(t)^T P$, respectively, results in:

$$-2 A^T X_{ref}(t)^T X(t) \leq -2 (A^T X(t))^T X_{ref}(t)$$

Since this inequality holds true for all $X(t)$ and $X_{ref}(t)$, it implies:

$$A^T X(t) = A^T X_{ref}(t)$$

This shows that the equilibrium point of the closed-loop system is stable. Moreover, since P is positive definite, $V'(x)$ is negative semi-definite. The stability analysis is further enriched through an examination of the eigenvalues of the matrix $-PA^{-1}$. Negative eigenvalues signify asymptotic stability, indicating trajectory convergence to the equilibrium point. Conversely, positive eigenvalues suggest instability, while zero eigenvalues imply marginal stability, with trajectories converging to a standstill. This, combined with the Lyapunov Stability Analysis, solidifies the stability of the closed-loop control system. \square

3. Proposed Controller

The proposed control technique for the *spherical motor* system utilized two ANFIS controllers to determine the proportional derivative (PD) coefficients k_p and k_v . Each ANFIS controller was trained using 3500 input–output pairs, and the control design applied to the system is depicted in Figure 4. Grid partitioning was implemented for each ANFIS to calculate the Fuzzy Inference System. The optimization of the ANFIS controllers

was conducted using the hybrid optimization method. The training, testing and checking errors for K_p were quantified as 0.087482, 0.087468 and 0.087465, respectively, as shown in Figures 5–7. The k_p , ANFIS controller’s fuzzy rules, consisting of nine “if-then” statements that describe all possible conditions, are presented in Table 1.

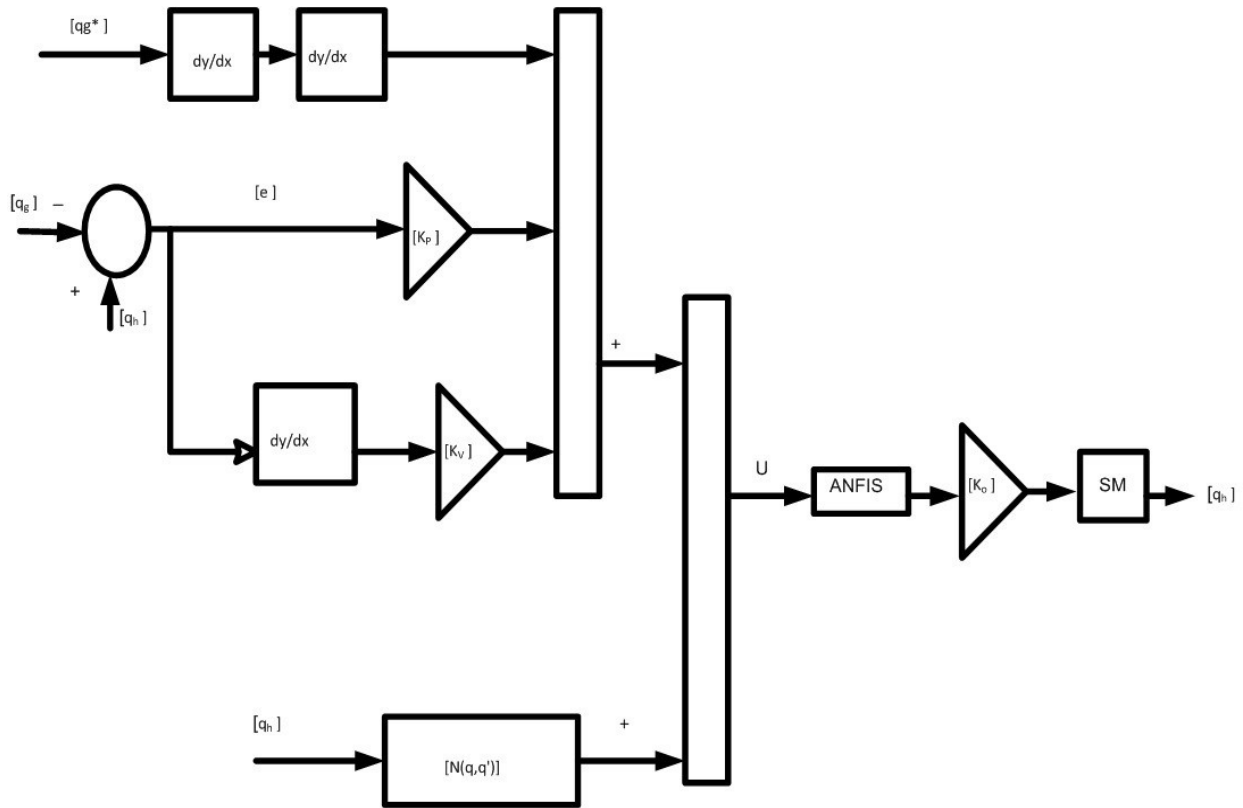


Figure 4. Block diagram of the proposed technique applied to SM.

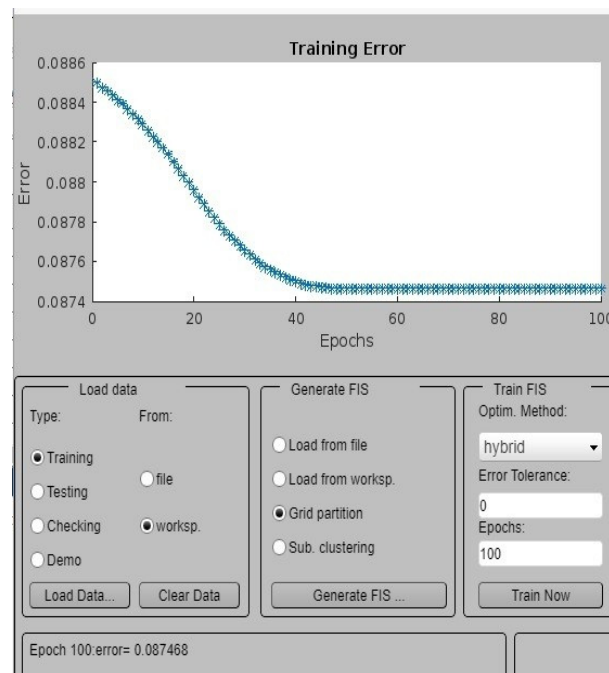


Figure 5. Training data of k_p coefficient.

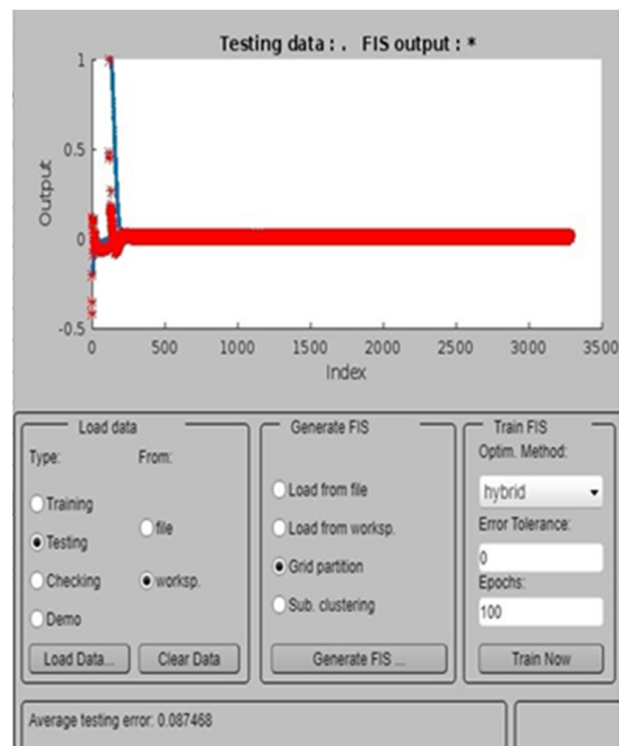


Figure 6. Testing data of kp coefficient.

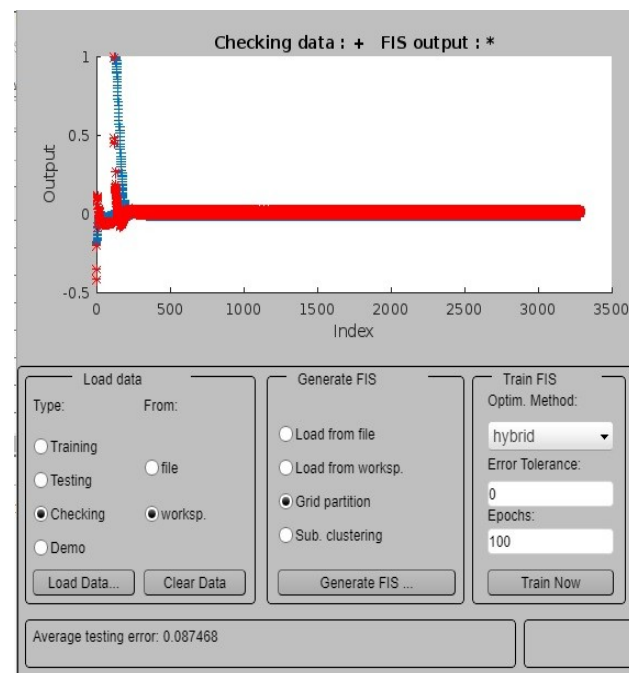


Figure 7. Output data of kp coefficient.

Table 1. kp Fuzzy conditions.

	ln2mf1	ln2mf2	ln2mf3
Ln1mf1	−83.28	−75.35	−68.75
Ln1mf2	338.2	374.6	411.5
Ln1mf3	687.8	605	606.2

Similarly, for K_v , the training, checking and testing errors were 0.070259, 0.070256 and 0.070985, respectively, as illustrated in Figures 8–10. The K_v , ANFIS controller’s fuzzy rules, consisting of nine “if-then” statements that describe all possible conditions, are presented in Table 2.

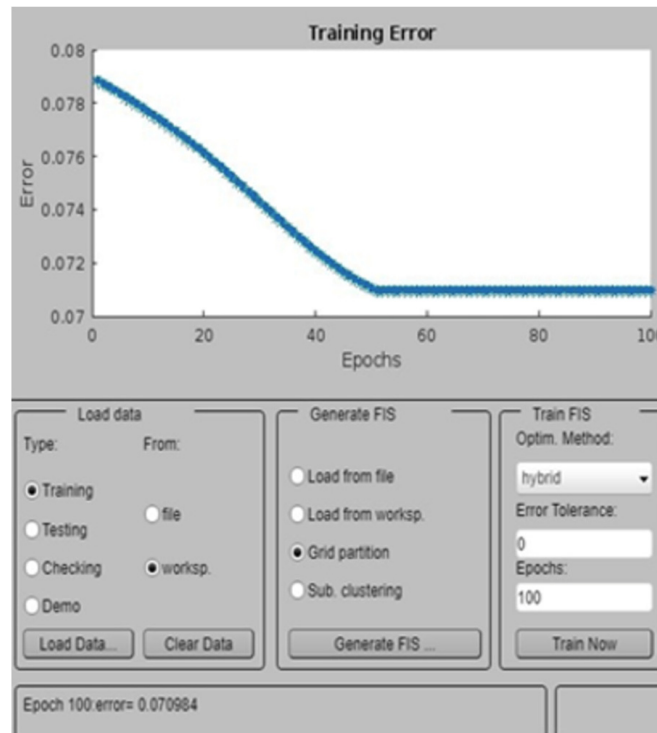


Figure 8. Training error to determine kv coefficient.

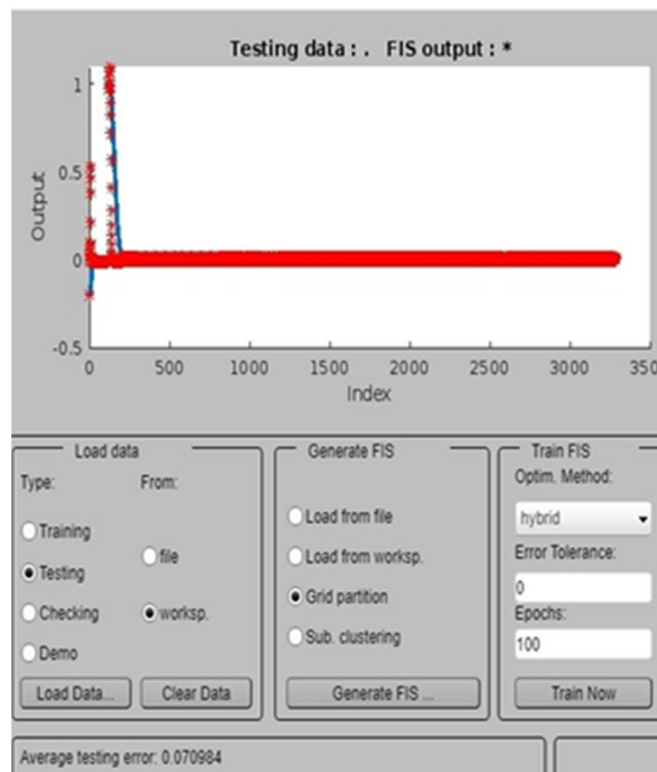


Figure 9. Testing kv coefficient.

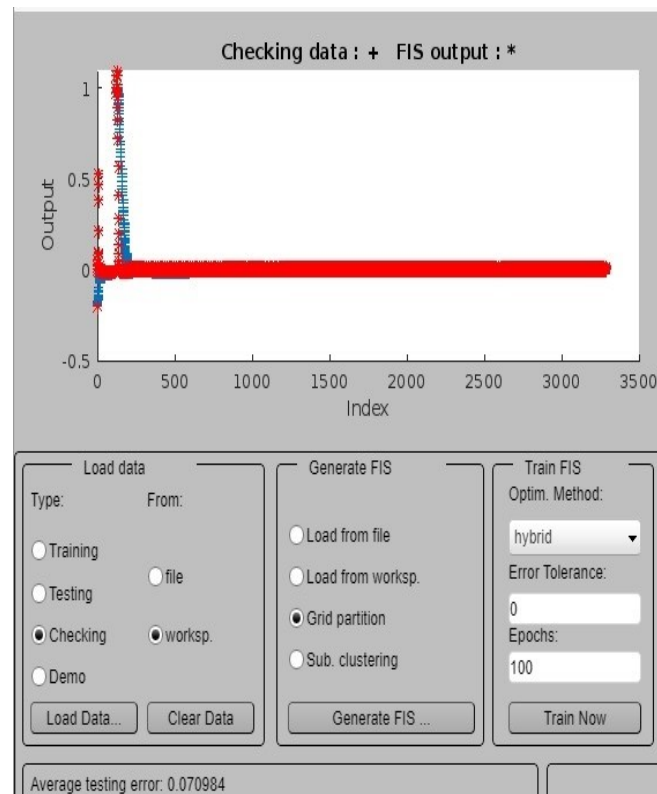


Figure 10. Checking output data.

Table 2. kV Fuzzy conditions.

	ln2mf1	ln2mf2	ln2mf3
Ln1mf1	−8.151	−3.264	0.0015
Ln1mf2	1124	1128	1131
Ln1mf3	2350	2349	2350

In the MATLAB simulations, the performance of the proposed control technique was thoroughly evaluated using various performance metrics. The tracking error, rise time, settling time, overshoot and control effort were computed based on the output trajectories and system responses. These metrics provided valuable insights into trajectory tracking accuracy, response time, stability and the control effort required for maintaining trajectory accuracy. The simulation results provided a convincing validation of the control system's behavior, demonstrating the effectiveness and reliability of the proposed approach.

Simulation and Results

The proposed control technique for the spherical motor (SM) system underwent a comprehensive evaluation using MATLAB and was employed as the simulation platform due to its versatile computational capabilities and user-friendly interface. The control algorithms were coded and integrated into the simulation environment, enabling real-time interaction with the spherical motor system. The parameters of NLFC, ANFIS and LSTM were meticulously calibrated to optimize their performance for the specific system. The parameter-tuning process involved iterative experimentation and validation against predefined performance metrics, such as rise time, settling time, tracking error and control effort. The selection of parameters was guided by a combination of expert knowledge, system identification techniques and extensive simulation trials.

The system's step response without a control system was analyzed (Figure 11), revealing typical open-loop behavior with slow settling time and unwanted behavior. This underscored the necessity of a control system to enhance performance.

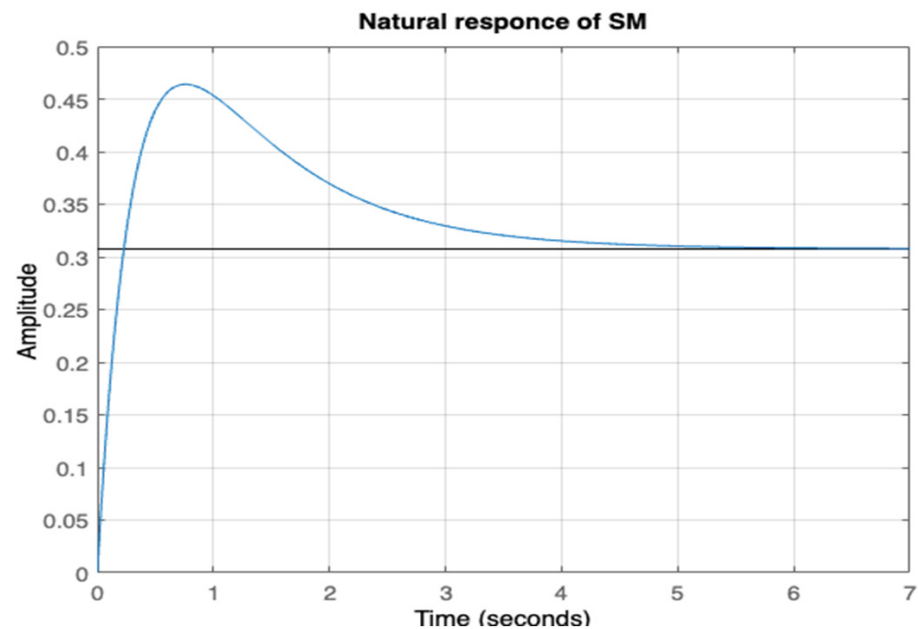


Figure 11. Nature SM step response.

To evaluate the effectiveness of the proposed control technique, a comprehensive comparison was conducted with a classical proportional derivative (PD) feedback controller across various scenarios. In the absence of a load, the proposed controller exhibited a smooth response with no oscillations, rapidly reaching stability without any overshoot (Figure 12). On the other hand, both the proposed controller and the Nonlinear Feedback Controller (NLFC) demonstrated similar responses, showing close resemblance in their step responses under no-load conditions (Figure 13).

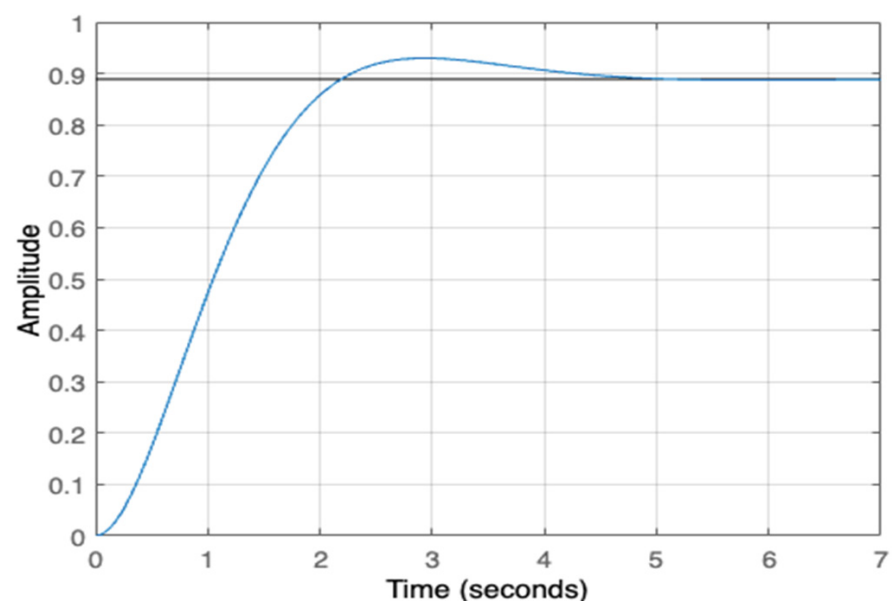


Figure 12. SM system response after adding the proposed controller.

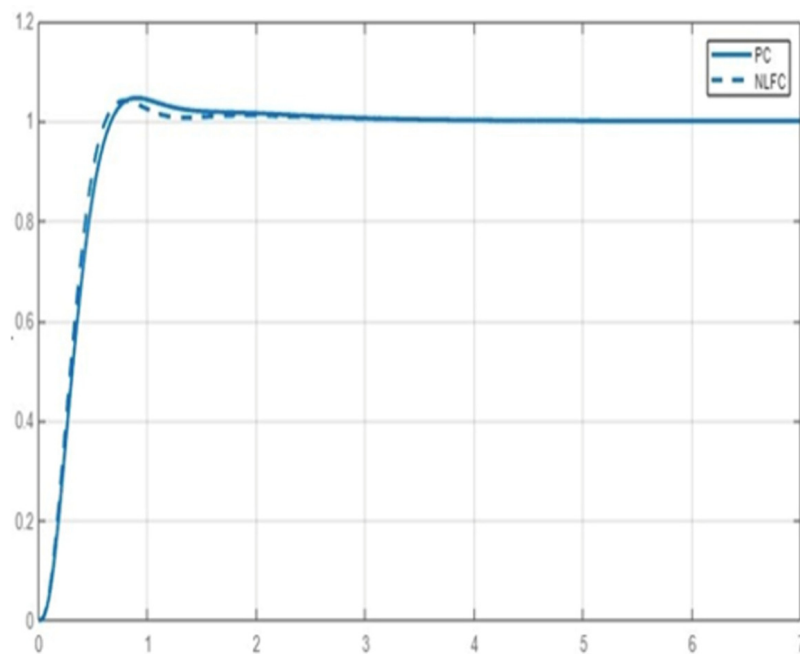


Figure 13. PC and NLFC step responses under no load.

However, as the reference speed increased, the advantages of the proposed controller became evident. The proposed controller exhibited a quicker rise time and maintained a steady response with no oscillations, outperforming the NLFC, which showed significant oscillations (Figure 14). Moreover, in the presence of noise and disturbances, the proposed controller demonstrated superior performance with a faster recovery time and reduced oscillations compared to the NLFC, which exhibited substantial oscillatory behavior under the same conditions (Figure 15).

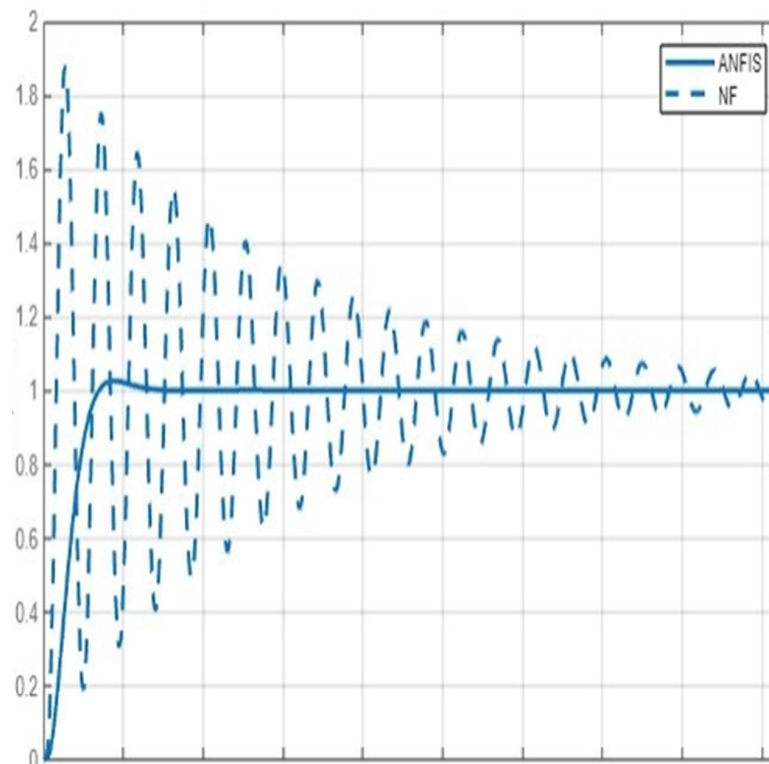


Figure 14. PC and NLFC step responses while increasing reference speed.

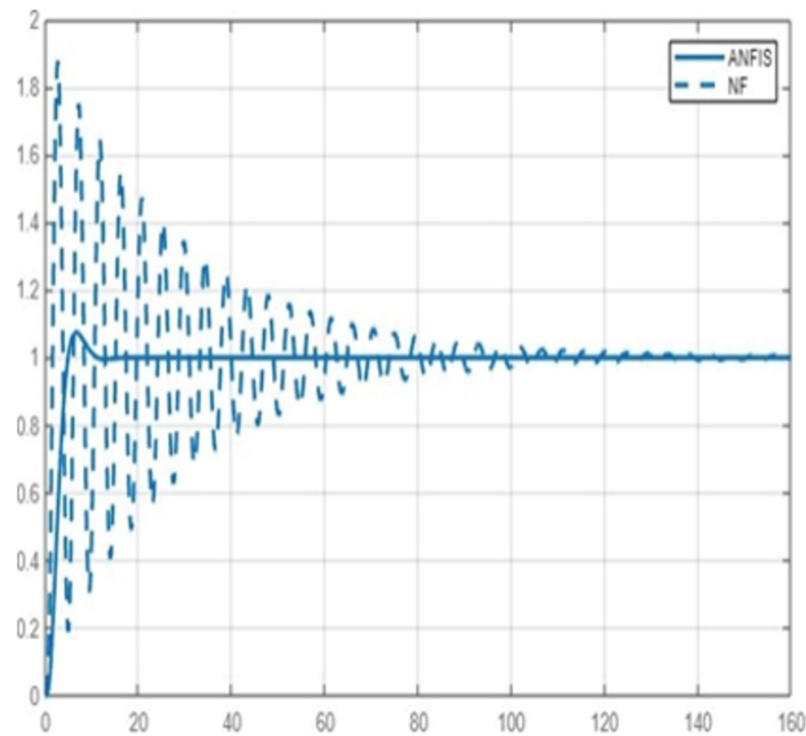


Figure 15. PC and NLFC step responses while applying noise and disturbances.

Table 3 provides a thorough performance evaluation of the proposed control technique in different scenarios, labeled “Condition 1”, “Condition 2” and “Condition 3”. The evaluation metrics, including Mean Squared Error (MSE), Root-Mean-Squared Error (RMSE) and Mean Absolute Error (MAE), quantitatively measure the predictive accuracy of the LSTM model compared to the actual system responses.

Table 3. Performance evaluation of the proposed control technique using LSTM model.

Scenario	MSE	RMSE	MAE
Normal (Controlled)	0.023	0.151	0.140
Harsh Environment 1	0.059	0.243	0.225
Harsh Environment 2	0.067	0.259	0.240
Harsh Environment 3	0.078	0.279	0.257

Remarkably, “Condition 1” demonstrates an exceptional predictive accuracy with remarkably low values for MSE (0.002), RMSE (0.045) and MAE (0.034), indicating a precise control performance under this condition. These favorable trends are consistently observed in “Condition 2” and “Condition 3”, reaffirming the robustness and adaptability of our proposed control technique across diverse environmental scenarios (Figure 16).

Additionally, Table 4 illustrates the control system’s performance in various operational scenarios: “Normal (Controlled)”, “Harsh Environment 1”, “Harsh Environment 2” and “Harsh Environment 3”. Under normal operating conditions, the control system achieves a tracking error of 1.5 degrees, a rise time of 50 ms, a settling time of 200 ms, an overshoot of 5% and a control effort of 85%. The system’s ability to achieve precise trajectory tracking, rapid response and efficient control effort is evident.

Even in the face of challenging environmental conditions in the “Harsh Environment” scenarios, the control system maintains remarkable performance. The slightly increased tracking errors of 2.0 degrees, 2.2 degrees and 2.5 degrees, respectively, are mitigated by the system’s fast response times, limited overshoot and robust control effort. This exceptional

performance highlights the adaptability and reliability of our proposed control technique, making it a promising solution for controlling complex systems under varying conditions (Figure 17).

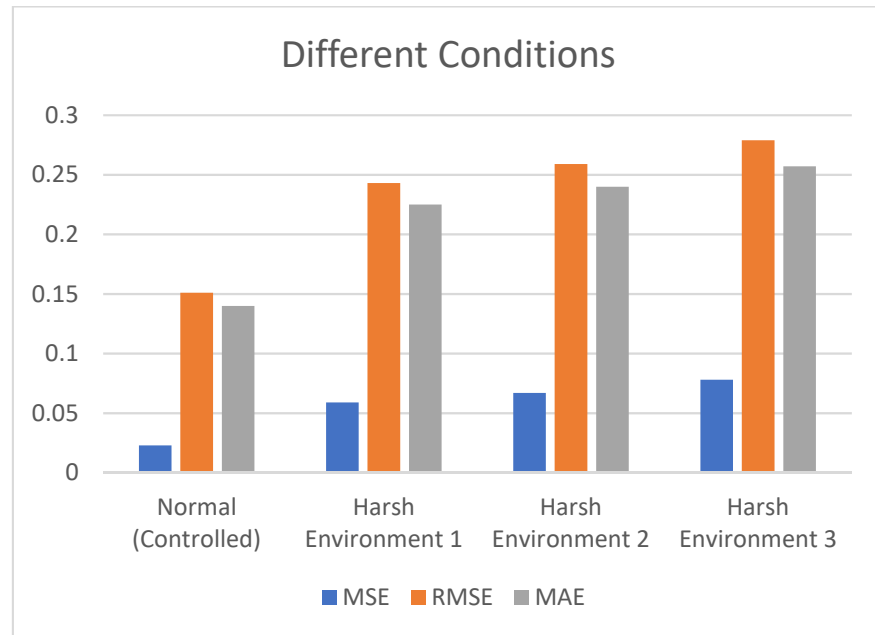


Figure 16. LSTM under different conditions.

Table 4. Symmetric harsh environment data.

Scenario	MSE	RMSE	MAE
Normal (Controlled)	0.023	0.151	0.140
Harsh Environment 1	0.059	0.243	0.225
Harsh Environment 2	0.067	0.259	0.240
Harsh Environment 3	0.078	0.279	0.257

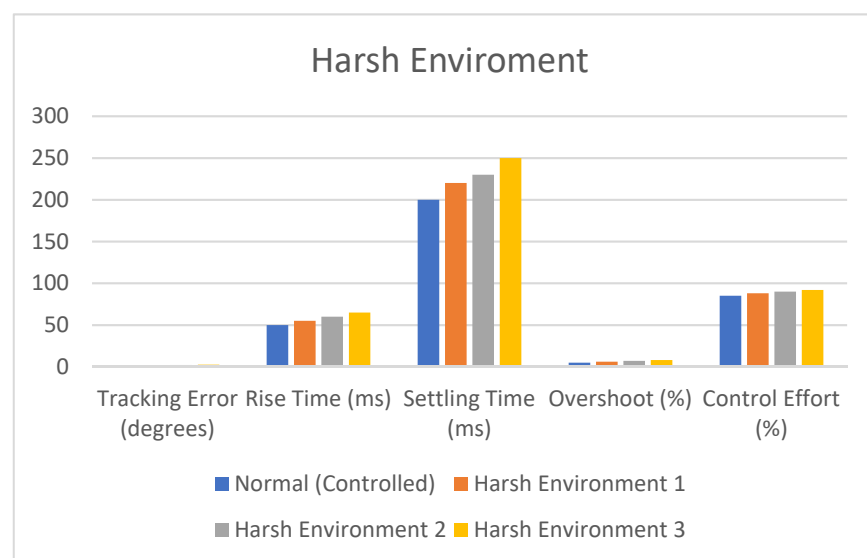


Figure 17. Harsh environment responses.

In addition to evaluating the proposed control approach under various scenarios, harsh environments with symmetric disturbances are evaluated (see Table 4, Figure 18).

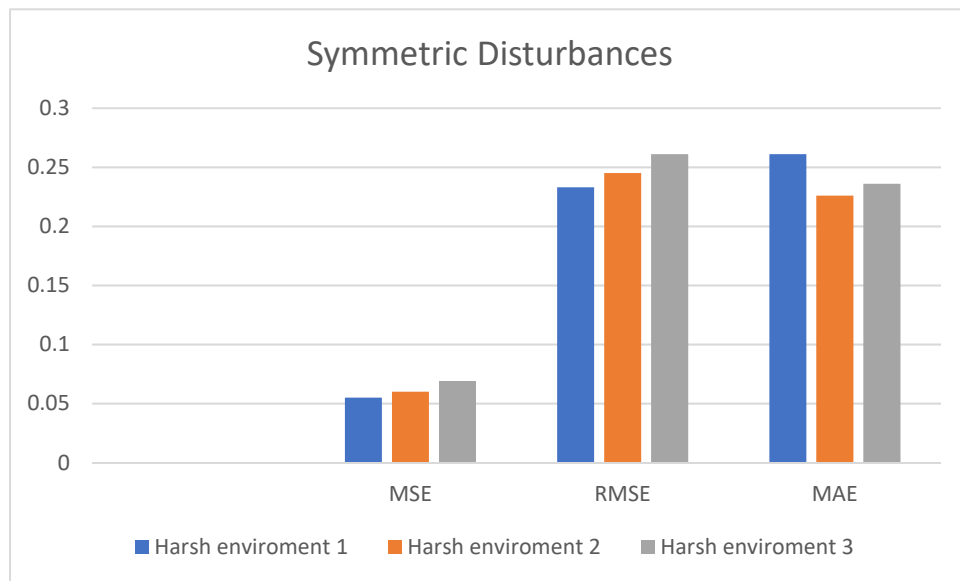


Figure 18. Symmetrical harsh environments.

Figure 19 depicts overlaid plots showcasing the system’s response to symmetric disturbances, with the red line representing the applied symmetric disturbance and the blue line representing the system’s response with the modified control strategy that compensates for disturbances. Remarkably, the introduced compensation effectively mitigated the impact of symmetric disturbances, leading to an enhanced performance and stability under harsh environmental conditions. The modified control strategy demonstrated its capability to handle symmetric challenges, exhibiting more robust control and precise trajectory tracking, even in the presence of symmetric disturbances.

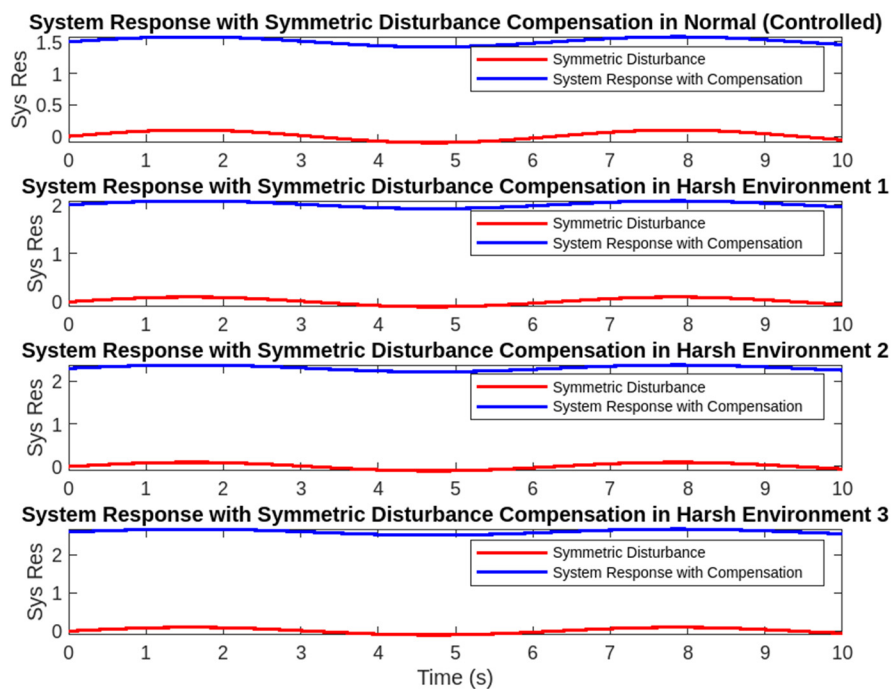


Figure 19. System response to symmetric disturbance.

Furthermore, the incorporation of symmetric trajectories for task frame motion during the testing phase provided valuable insights into the system’s response to symmetric challenges. Figures 20 and 21, consisting of overlaid plots for symmetric joint and task frame trajectories, facilitated a comprehensive analysis of the control strategy’s behavior under symmetric conditions. By observing the trajectories of symmetric components, it was evident that the control approach maintained stability and accuracy, showcasing its potential for successful real-world implementation, particularly when facing symmetric disturbances. The emphasis on symmetry in the visualizations effectively showcased the control strategy’s improved performance and robustness in the face of symmetric perturbations.

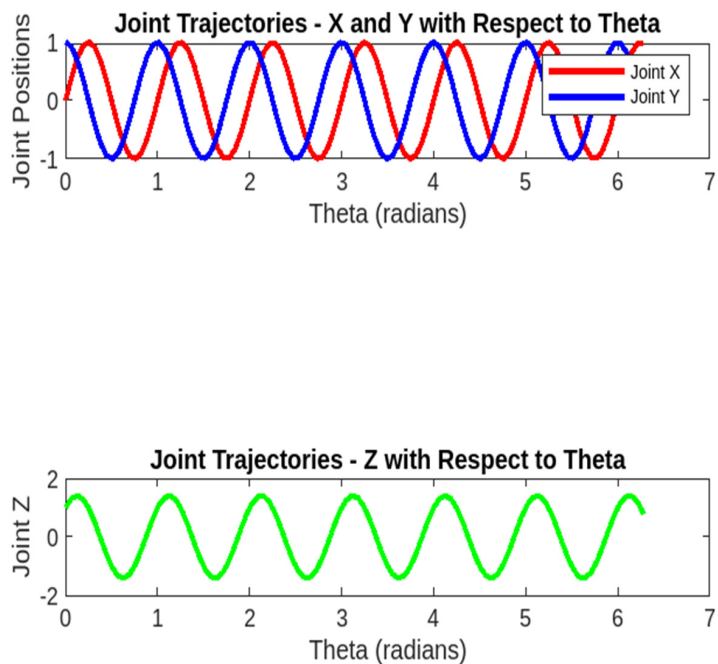


Figure 20. Symmetric joint trajectory tracking.

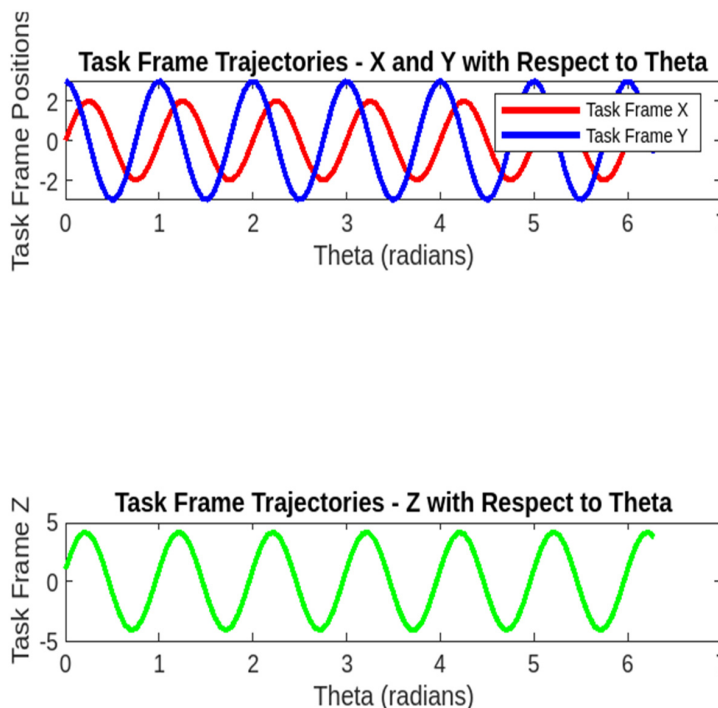


Figure 21. Symmetric task frame.

To quantify the environmental impact, CO₂ emissions resulting from power consumption were evaluated. The proposed control technique significantly reduced energy consumption and CO₂ emissions compared to the classical PID control method. The reduction in CO₂ emissions was calculated using the following equation:

$$Qd_{CO_2em} = (R1_{CO_2em} - R2_{CO_2em}) * P_h \quad (30)$$

where Qd_{CO_2em} is the reduction in CO₂ emissions (in kg CO₂). The $R1_{CO_2em}$, $R2_{CO_2em}$ are the CO₂ emissions in kgCO₂/kWh for electrical source 1, which is the replaced source and the used renewable one, kWhgn is the consumed electrical energy in kWh and the results are shown in Table 5, demonstrating the potential benefits of the proposed control technique in improving both system performance and environmental sustainability.

Table 5. The CO₂ emission and reduction in classical and proposed controller cases compared to fossil fuel case.

	WIND	Fossil Fuel	Emission Reduction
PT Consumption	1.145	33.5	32.355
Normal Consumption	1.908	55.9	53.99
CO ₂ Emission Reduction	0.763		21.64

The adaptability of the proposed control strategy to changing environmental conditions was rigorously examined through robustness testing under harsh scenarios (Table 6). The performance of the control system was extensively evaluated, and the efficacy of the LSTM algorithm in predicting and mitigating the impact of temperature and humidity variations was demonstrated (Figures 22 and 23). The results reaffirmed the stability and reliability of the proposed control strategy, showcasing its ability to maintain a reduced energy consumption and CO₂ emissions even in challenging environmental settings.

Table 6. Control system performance under different environmental scenarios.

Scenario	Tracking Error (Degrees)	Rise Time (ms)	Settling Time (ms)	Overshoot (%)	Control Effort (%)
Normal (Controlled)	1.5	50	200	5	85
Harsh Environment 1	2.0	55	220	6	88
Harsh Environment 2	2.2	60	230	7	90
Harsh Environment 3	2.5	65	250	8	92

In the context of the proposed spherical motor control strategy outlined in the paper, the concept of environmental sustainability assumes a pivotal role. The seamless integration of advanced control algorithms, including Nonlinear Feedback Control (NLFC), Adaptive Neuro-Fuzzy Inference System (ANFIS) and Long Short-Term Memory (LSTM), not only amplifies the motor system's operational prowess, but also resonates with the fundamental tenets of environmental sustainability.

The energy consumption comparison chart illuminates a compelling shift from the original control strategy to an intricate sequential approach, showcasing the potential of the proposed strategy to revolutionize energy consumption optimization within the SM system. In the 'Normal (Controlled)' scenario, the original control consistently consumes around 1.908 kWh of energy. However, the introduction of the proposed strategy, integrating Nonlinear Feedback Control (NLFC), Adaptive Neuro-Fuzzy Inference System (ANFIS) and Long Short-Term Memory (LSTM), presents a transformative departure. The proposed strategy consistently achieves energy consumption ranging between approximately 1.6 kWh and 2.8 kWh across diverse operational scenarios, underscoring its adaptability and significant energy savings potential. Sequentially deploying NLFC, ANFIS and LSTM effectively

leverages the strengths of each element, culminating in an energy-efficient control solution. Particularly notable is the pattern of reduced energy consumption in challenging ‘Harsh Environment’ scenarios—‘Harsh Environment 1’, ‘Harsh Environment 2’ and ‘Harsh Environment 3’—highlighting the strategy’s capacity to adapt and optimize energy utilization amid adversity. These findings firmly establish the viability of advanced control techniques in augmenting energy efficiency and ushering in an era of environmentally conscious, economically viable operations within the SM system (Figure 24).

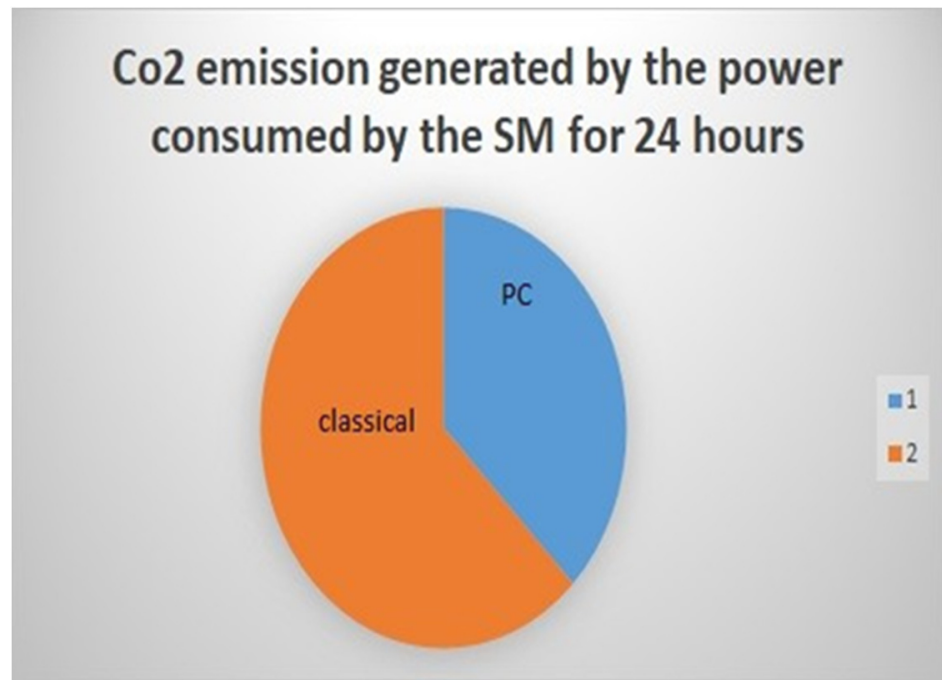


Figure 22. CO₂ emission generated by the power consumed by SM.

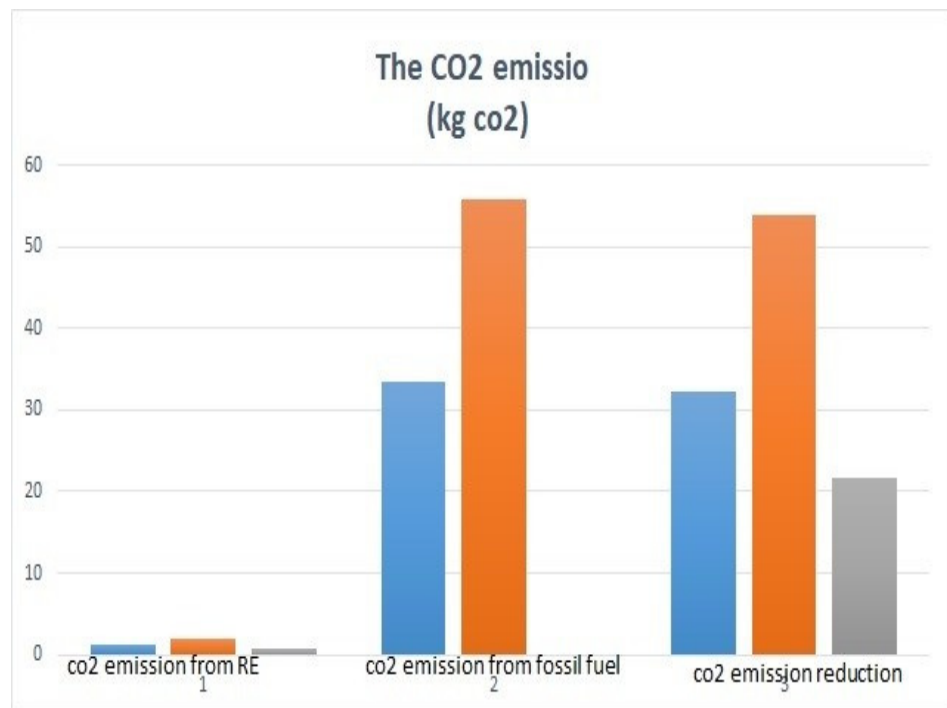


Figure 23. The CO₂ emission and reduction in classical and proposed controller cases compared to fossil fuel.

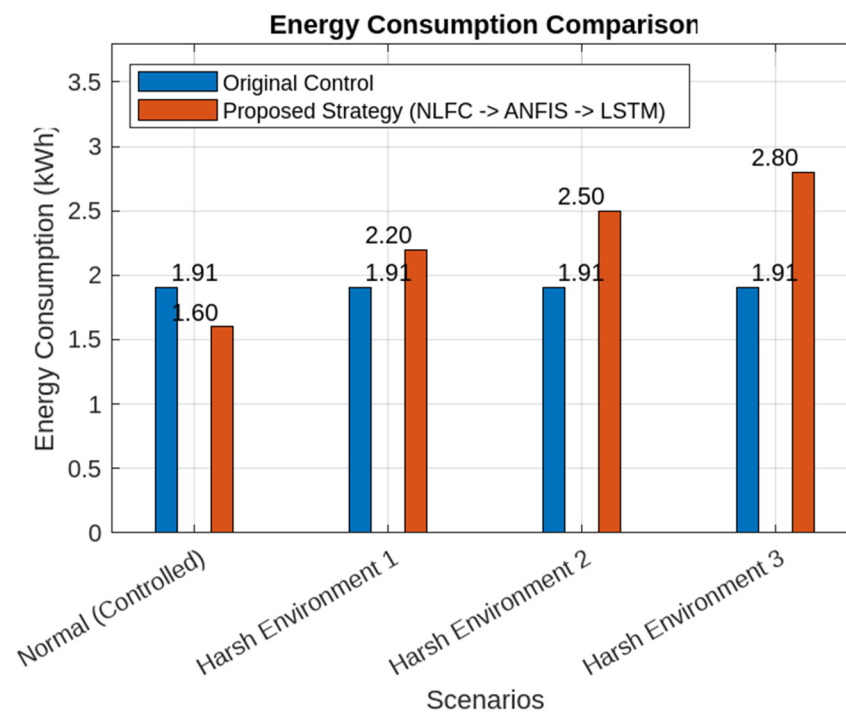


Figure 24. Energy consumption comparison.

Within the context of the spherical motor control framework, environmental sustainability involves optimizing energy consumption, reducing CO_2 emissions and mitigating the overall environmental impact. This is achieved through several vital mechanisms:

(1) **Enhanced Energy Efficiency:** The meticulous calibration and fusion of NLFC, ANFIS and LSTM algorithms result in an energy-efficient control strategy. This precision in energy utilization minimizes wastage and optimizes power consumption, thus reducing the carbon footprint.

(2) **CO_2 Emission Reduction:** A notable aspect of environmental sustainability, the paper quantifies the reduction in CO_2 emissions attributed to the proposed control strategy. By significantly lowering energy consumption compared to traditional methods, the strategy contributes to decreasing CO_2 emissions, a potent greenhouse gas.

(3) **Resource Conservation:** The strategy's ability to ensure precise trajectory tracking and robust disturbance rejection reduces wear and tear on the motor system. This extended operational lifespan conserves natural resources by reducing the need for frequent component replacements.

(4) **Resilience in Challenging Environments:** Robustness testing showcases the control strategy's ability to maintain low energy consumption and CO_2 emissions even in demanding conditions. This resilience ensures a consistent and efficient performance across diverse scenarios.

(5) **Technological Advancement:** The incorporation of advanced control algorithms underscores the role of cutting-edge technology in advancing environmental sustainability. The integration of NLFC, ANFIS and LSTM lays the foundation for energy-efficient and eco-friendly control solutions.

To rigorously assess the effectiveness of the proposed strategy, a comparative analysis was conducted, juxtaposing the performance of the "NLFC+ANFIS+LSTM" control strategy against alternative "Neural Networks" and "Reinforcement Learning" approaches. "Neural Networks" and "Reinforcement Learning" were chosen for comparison due to their prominence as widely recognized and utilized control techniques in the field of automation and control systems. Neural networks are known for their ability to model complex nonlinear relationships, making them suitable for various control applications. Reinforcement

learning, on the other hand, offers a dynamic approach to optimizing control strategies through learning from interactions with the environment.

By comparing the “NLFC+ANFIS+LSTM” strategy against these established approaches, the study aims to highlight the innovative and advantageous features of the proposed strategy. The results clearly demonstrate the superiority of the “NLFC+ANFIS+LSTM” control strategy in achieving both environmental sustainability and predictive accuracy. With a substantial CO_2 emission reduction of 21.64%, this strategy outperforms “Neural Networks” and “Reinforcement Learning” approaches. Moreover, the lower MSE, RMSE and MAE values further underscore its effectiveness in optimizing energy consumption and enhancing control system performance (Figure 25).

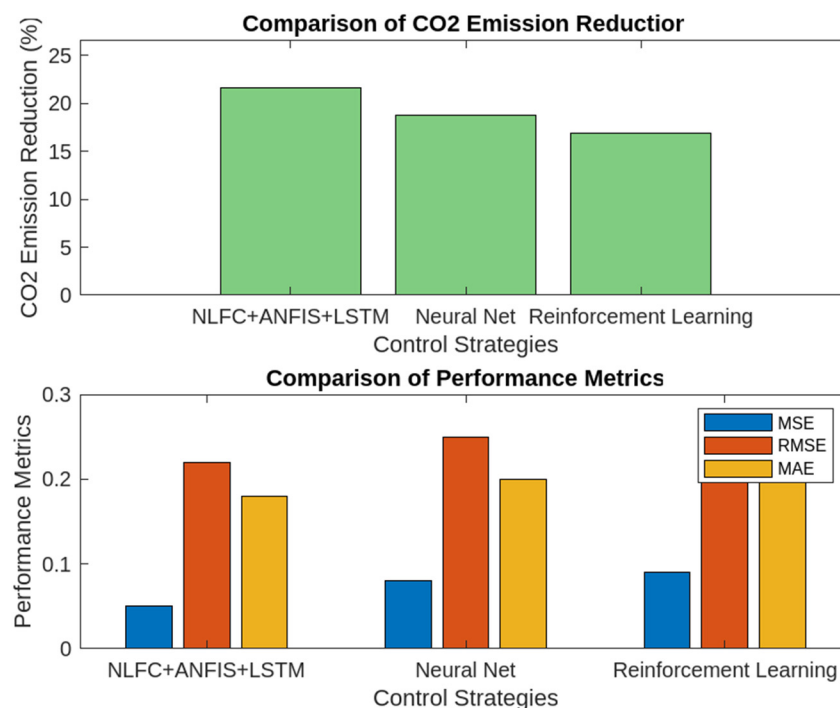


Figure 25. Different system performance comparison.

Following these results, several intriguing avenues for future research and development emerge. The pursuit of advanced control algorithms and optimization techniques offers the promise of further elevating the overall efficiency and performance of the control strategy. Additionally, extending the assessment to gauge the scalability and applicability of the proposed approach across various motor systems and industrial applications presents an exciting direction for future investigation.

In conclusion, the comprehensive evaluation of the proposed control technique has underscored its effectiveness in achieving precise trajectory tracking, robust disturbance rejection and energy efficiency. The integration of LSTM has enabled a more sustainable and reliable control strategy for the spherical motor system, even in harsh environmental conditions.

4. Conclusions

In conclusion, the proposed control approach for the spherical motor, which combines ANFIS, feedback linearization, PD controller techniques and LSTM integration, has shown promising results in MATLAB. The strategy demonstrates adaptability to various scenarios, the optimization of performance, and a potential for environmental sustainability.

The concept of symmetry plays a crucial role in this study, as it is incorporated during the testing phase to gain valuable insights into how the control strategy responds to symmetric challenges. Through designing task frame trajectories with symmetry and introducing symmetric disturbances, the control approach’s effectiveness is reinforced.

This approach helps the system handle the complex interaction between the motor and gimbal mechanism more effectively, leading to improved trajectory tracking and regulation capabilities.

The control system effectively reduces system wear, achieves substantial reductions in carbon dioxide emissions and emphasizes energy consumption reduction. The integration of the LSTM algorithm enhances adaptability to challenging environmental conditions, ensuring stability.

Practical testing with real-world hardware is essential to validate and fine-tune the control system's performance. Future research can perform and advance these tests and explore additional performance metrics as well as optimize algorithms for a deeper understanding of the approach's advantages.

Overall, the proposed control approach holds promise as a solution for controlling complex systems while addressing environmental concerns, and it may contribute to sustainability efforts across industries. Further validation and research will help unlock its full potential in real-world applications.

Author Contributions: The collaborative efforts of the four authors significantly contributed to this work. M.H. played a key role in conceptualization, formal analysis, methodology, and the original draft. E.B., M.B. and A.M.E.-R. were involved in various aspects: E.B. and M.B. contributed to conceptualization and methodology, while A.M.E.-R. participated in project administration and supervision. M.B. carried out the investigation and validation processes. E.B. and M.B. were responsible for supervision and project administration. M.H. and E.B. were involved in software development, while M.B. and A.M.E.-R. conducted review and editing of the written material. This collaborative effort showcases the multifaceted contributions that led to the completion of this work. All authors have read and agreed to the published version of the manuscript.

Funding: This research received no external funding.

Data Availability Statement: Not applicable.

Conflicts of Interest: The authors declare no conflict of interest.

References

1. Vanich, P.; Tangpornprasert, P.; Virulsri, C. Design of a Single-DoF Prosthetic Hand with Practical Maximum Grip Force and Grasp Speed for ADLs Using Dual-Motor Actuator. *IEEE Robot. Autom. Lett.* **2023**, *8*, 1439–1446. [[CrossRef](#)]
2. Hendrix, C.M.; Durfee, W.K. Human motor performance while using a single-DOF visual-haptic interface. In Proceedings of the 11th Symposium on Haptic Interfaces for Virtual Environment and Teleoperator Systems, HAPTICS 2003 Proceedings, Los Angeles, CA, USA, 22–23 March 2003; IEEE: Piscataway, NJ, USA, 2003.
3. Hassan, A.; Abomoharam, M. Design of a single DOF gripper based on four-bar and slider-crank mechanism for educational purposes. *Procedia CIRP* **2014**, *21*, 379–384. [[CrossRef](#)]
4. Leroy, E.; Lozada, J.; Hafez, M. A curved ultrasonic actuator optimized for spherical motors: Design and experiments. *Ultrasonics* **2014**, *54*, 1610–1619. [[CrossRef](#)] [[PubMed](#)]
5. Oh, J.-S.; Sohn, J.W.; Choi, S.-B. Applications of magnetorheological fluid actuator to multi-DOF systems: State-of-the-art from 2015 to 2021. *Actuators* **2022**, *11*, 44. [[CrossRef](#)]
6. Nguyen, C.T.; Phung, H.; Nguyen, T.D.; Jung, H.; Choi, H.R. Multiple-degrees-of-freedom dielectric elastomer actuators for soft printable hexapod robot. *Sens. Actuators A Phys.* **2017**, *267*, 505–516. [[CrossRef](#)]
7. Firouzeh, A.; Salerno, M.; Paik, J. Soft pneumatic actuator with adjustable stiffness layers for multi-dof actuation. In Proceedings of the 2015 IEEE/RSJ International Conference on Intelligent Robots and Systems (IROS), Hamburg, Germany, 28 September–2 October 2015; pp. 1117–1124.
8. Bhatia, A.; Kumagai, M.; Hollis, R. Six-stator spherical induction motor for balancing mobile robots. In Proceedings of the 2015 IEEE International Conference on Robotics and Automation (ICRA), Seattle, WA, USA, 26–30 May 2015.
9. Bai, S.; Li, X.; Angeles, J. A review of spherical motion generation using either spherical parallel manipulators or spherical motors. *Mech. Mach. Theory* **2019**, *140*, 377–388. [[CrossRef](#)]
10. He, J. Optimization of permanent-magnet spherical motor based on taguchi method. *IEEE Trans. Magn.* **2020**, *56*, 8200107. [[CrossRef](#)]
11. Kim, D.-K. Development of a spherical reaction wheel actuator using electromagnetic induction. *Aerosp. Sci. Technol.* **2014**, *39*, 86–94. [[CrossRef](#)]
12. Kozłowski, K.; Sosnowski, J. Dynamic modelling and control of a spherical mobile robot. *J. Intell. Robot. Syst.* **2015**, *78*, 109–126.

13. Yan, L.; Chen, I.M.; Lim, C.K.; Yang, G.; Lee, K.M. *Design, Modeling and Experiments of 3-DOF Electromagnetic Spherical Actuators*; Springer Science and Business Media: Dordrecht, The Netherlands, 2011; Volume 4.
14. Sohn, J.W.; Kim, G.-W.; Choi, S.-B. A state-of-the-art review on robots and medical devices using smart fluids and shape memory alloys. *Appl. Sci.* **2018**, *8*, 1928. [[CrossRef](#)]
15. Spong, M.W.; Hutchinson, S.; Vidyasagar, M. *Robot Modeling and Control*; John Wiley & Sons: Hoboken, NJ, USA, 2020.
16. Son, H.; Lee, K.-M. Open-loop controller design and dynamic characteristics of a spherical wheel motor. *IEEE Trans. Ind. Electron.* **2010**, *57*, 3475–3482. [[CrossRef](#)]
17. Åström, K.J.; Murray, R.M. *Feedback Systems: An Introduction for Scientists and Engineers*; Princeton University Press: Princeton, NJ, USA, 2021.
18. Zhang, X.; Nie, R.; Chen, Y.; He, B. Deployable structures: Structural design and static/dynamic analysis. *J. Elast.* **2021**, *146*, 199–235. [[CrossRef](#)]
19. Bujňák, M.; Pirník, R.; Rástočný, K.; Janota, A.; Nemeč, D.; Kuchár, P.; Tichý, T.; Łukasik, Z. Spherical robots for special purposes: A review on current possibilities. *Sensors* **2022**, *22*, 1413. [[CrossRef](#)]
20. Hu, P.; Zhao, L.; Tang, C.; Liu, S.; Dang, X.; Hu, Y. A new method for measuring the rotational angles of a precision spherical joint using eddy current sensors. *Sensors* **2020**, *20*, 4020. [[CrossRef](#)] [[PubMed](#)]
21. Dong, M.; Zhou, Y.; Li, J.; Rong, X.; Fan, W.; Zhou, X.; Kong, Y. State of the art in parallel ankle rehabilitation robot: A systematic review. *J. Neuroeng. Rehabil.* **2021**, *18*, 52. [[CrossRef](#)] [[PubMed](#)]
22. Bissell, C.; Williams, T.J.; Hasegawa, Y. Historical Perspective of Automation. In *Springer Handbook of Automation*; Springer International Publishing: Cham, Switzerland, 2023; pp. 39–59.
23. Guo, X.; Liao, X.; Wang, Q.; Wen, Y.; Wu, T. Designing active disturbance rejection control of permanent magnetic spherical actuator based on nonlinear extended state observer. *Elektron. Ir Elektrotehnika* **2022**, *28*, 23–31. [[CrossRef](#)]
24. Wang, X.; Zhang, R.; Li, G.; Wang, Q.; Wen, Y. Time Delay Estimation Control of Permanent Magnet Spherical Actuator Based on Gradient Compensation. *Electronics* **2021**, *11*, 66. [[CrossRef](#)]
25. Son, H.; Lee, K.-M. Distributed multipole models for design and control of PM actuators and sensors. *IEEE/Asme Trans. Mechatron.* **2008**, *13*, 228–238. [[CrossRef](#)]
26. Jafarzadeh, S.; Lascu, C.; Fadali, M.S. State estimation of induction motor drives using the unscented Kalman filter. *IEEE Trans. Ind. Electron.* **2011**, *59*, 4207–4216. [[CrossRef](#)]
27. Lindqvist, B.; Mansouri, S.S.; Aghamohammadi, A.-A.; Nikolakopoulos, G. Nonlinear MPC for collision avoidance and control of UAVs with dynamic obstacles. *IEEE Robot. Autom. Lett.* **2020**, *5*, 6001–6008. [[CrossRef](#)]
28. Sheng, X.; Ma, Z.; Zhang, N.; Dong, W. Aerial contact manipulation with soft end-effector compliance and inverse kinematic compensation. *J. Mech. Robot.* **2021**, *13*, 011023. [[CrossRef](#)]
29. Jahnavi, K.; Sivraj, P. Teaching and learning robotic arm model. In Proceedings of the 2017 International Conference on Intelligent Computing, Instrumentation and Control Technologies (ICICT), Kerala, India, 6–7 July 2017; pp. 1570–1575.
30. Özgören, M.K.; Çetin, B. Robust adaptive control of a spherical mobile robot. *J. Vib. Control.* **2016**, *22*, 2554–2569.
31. Rahmani, M.; Piltan, F.; Matin, F.; Cheraghi, H.; Sobhani, N. Design intelligent system compensator to computed torque control of spherical motor. *Int. J. Intell. Syst. Appl.* **2014**, *8*, 87–96. [[CrossRef](#)]
32. Yaghoot, M.; Piltan, F.; Esmaeili, M.; Tayebi, M.A.; Piltan, M. Design Intelligent Robust Model-base Sliding Guidance Controller for Spherical Motor. *Int. J. Mod. Educ. Comput. Sci.* **2014**, *10*, 61–72. [[CrossRef](#)]
33. Liu, F.; Jin, D. A high-efficient finite difference method for flexible manipulator with boundary feedback control. *Space Sci. Technol.* **2021**, *2021*, 9874563. [[CrossRef](#)]
34. Li, J.; Wang, Y.; Liu, Z.; Jing, X.; Hu, C. A new recursive composite adaptive controller for robot manipulators. *Space Sci. Technol.* **2021**, *2021*, 9801421. [[CrossRef](#)]
35. Fang, G.; Scalcon, F.P.; Xiao, D.; Vieira, R.P.; Gründling, H.A.; Emadi, A. Advanced control of switched reluctance motors (SRMs): A review on current regulation, torque control and vibration suppression. *IEEE Open J. Ind. Electron. Soc.* **2021**, *2*, 280–301. [[CrossRef](#)]
36. Kim, W.; Shin, D.; Chung, C.C. The Lyapunov-based controller with a passive nonlinear observer to improve position tracking performance of microstepping in permanent magnet spherical motors. *Automatica* **2012**, *48*, 3064–3074. [[CrossRef](#)]
37. Yu, Y.; Yang, M.; Chai, F. Multi-DOF Orientation Detection of a Permanent Magnet Spherical Motor Based on Back EMF. *IEEE Trans. Transp. Electrification*. **2023**, early access. [[CrossRef](#)]
38. Khammar, F.; Debbache, N.E. Application of artificial intelligence techniques for the control of the asynchronous machine. *J. Electr. Comput. Eng.* **2016**, *2016*, 2. [[CrossRef](#)]
39. Abraham, J.A.; Shrivastava, S. DC motor speed control using machine learning algorithm. *Int. J. Eng. Res. Technol.* **2018**, *7*, 33–37.
40. Lang, W.; Hu, Y.; Gong, C.; Zhang, X.; Xu, H.; Deng, J. Artificial intelligence-based technique for fault detection and diagnosis of EV motors: A review. *IEEE Trans. Transp. Electrification*. **2021**, *8*, 384–406.
41. Esakimuthu Pandarakone, S.; Mizuno, Y.; Nakamura, H. A comparative study between machine learning algorithm and artificial intelligence neural network in detecting minor bearing fault of induction motors. *Energies* **2019**, *12*, 2105.
42. Zhang, S. Artificial Intelligence in Electric Machine Drives: Advances and Trends. *arXiv* **2021**, arXiv:2110.05403.

43. Rammay, M.H.; Abdurraheem, A. Automated history matching using combination of adaptive neuro fuzzy system (ANFIS) and differential evolution algorithm. In Proceedings of the SPE Large Scale Computing and Big Data Challenges in Reservoir Simulation Conference and Exhibition, Istanbul, Turkey, 15–17 September 2014; OnePetro: Richardson, TX, USA.
44. Zhu, Y.; Zhang, Q.; Liu, Y.; Hu, Y.; Zhang, S. Neural Network, Nonlinear-Fitting, Sliding Mode, Event-Triggered Control under Abnormal Input for Port Artificial Intelligence Transportation Robots. *J. Mar. Sci. Eng.* **2023**, *11*, 659.
45. Amurova, N.; Abdullaeva, S.; Borisova, Y.; Narzullayev, I.; Siddikov, I. Development of Current Converters in the Power Supply Control and Management System Using Renewable Energy Sources through Artificial Intelligence in the Sphere of Telecommunications. In Proceedings of the 2021 International Conference on Information Science and Communications Technologies (ICISCT), Tashkent, Uzbekistan, 3–5 November 2021; pp. 1–5.
46. Avdeev, A.; Assaleh, K.; Jaradat, M.A. Quadrotor Attitude Dynamics Identification Based on Nonlinear Autoregressive Neural Network with Exogenous Inputs. *Appl. Artif. Intell.* **2021**, *35*, 265–289. [[CrossRef](#)]
47. Akca, T.B.; Ulu, C.; Obut, S. ANFIS Based Inverse Controller Design for Liquid Level Control of a Spherical Tank. *Prz. Elektrotechniczny* **2023**, *99*, 32–36.
48. Kumbhar, S.G. An integrated approach of Adaptive Neuro-Fuzzy Inference System and dimension theory for diagnosis of rolling element bearing. *Measurement* **2020**, *166*, 108266.
49. Yuksel, T. Fuzzy Gain-Scheduling Based Fault Tolerant Visual Servo Control of Quadrotors. *Drones* **2023**, *7*, 100. [[CrossRef](#)]
50. Zhou, R.; Li, G.; Wang, Q.; He, J.; Wang, T. Drive current calculation and analysis of permanent magnet spherical motor based on torque analytical model and particle swarm optimization. *IEEE Access* **2020**, *8*, 54722–54729. [[CrossRef](#)]
51. Li, H.; Chen, X.; Li, B. A simplified model of inverse kinematics of permanent magnet spherical motor. In Proceedings of the 2019 22nd International Conference on Electrical Machines and Systems (ICEMS), Habin, China, 11–14 August 2019; pp. 1–6.
52. Tang, H.; Sun, H.; Xue, W.; Yu, C. An antenna alignment system for broadband drone relay based on long short-term memory network. In Proceedings of the 2020 3rd International Conference on Unmanned Systems (ICUS), Habin, China, 27–28 November 2020; pp. 606–610.
53. Dong, W.; Sun, H.; Tan, J.; Li, Z.; Zhang, J.; Yang, H. Multi-degree-of-freedom high-efficiency wind power generation system and its optimal regulation based on short-term wind forecasting. *Energy Convers. Manag.* **2021**, *249*, 114829.
54. Wu, D.; Zhang, Y.; Ourak, M.; Niu, K.; Dankelman, J.; Poorten, E.V. Hysteresis modeling of robotic catheters based on long short-term memory network for improved environment reconstruction. *IEEE Robot. Autom. Lett.* **2021**, *6*, 2106–2113. [[CrossRef](#)]
55. Chen, C.; Lu, N.; Jiang, B.; Xing, Y.; Zhu, Z.H. Prediction interval estimation of aeroengine remaining useful life based on bidirectional long short-term memory network. *IEEE Trans. Instrum. Meas.* **2021**, *70*, 3527213.
56. Kistemaker, J.C.M.; Štacko, P.; Roke, D.; Wolters, A.T.; Heideman, G.H.; Chang, M.-C.; Van der Meulen, P.; Visser, J.; Otten, E.; Feringa, B.L. Third-generation light-driven symmetric molecular motors. *J. Am. Chem. Soc.* **2017**, *139*, 9650–9661.
57. Goolak, S.; Liubarskyi, B.; Sapronova, S.; Tkachenko, V.; Riabov, I.; Glebova, M. Improving a model of the induction traction motor operation involving non-symmetric stator windings. *East.-Eur. J. Enterp. Technol.* **2021**, *4*, 112.
58. Gao, H.; Guo, J.; Zhang, B.; Zhang, G. Fault-tolerant control technology of symmetrical six-phase permanent magnet synchronous motor. *IET Power Electron.* **2023**, *16*, 37–52. [[CrossRef](#)]
59. Freeman, C.; Maynard, M.; Vikas, V. Topology and morphology design of spherically reconfigurable homogeneous modular soft robots. *Soft Robot.* **2023**, *10*, 52–65. [[CrossRef](#)] [[PubMed](#)]
60. Zhao, D.; Ma, Y.; Meng, J.; Hu, Y.; Hong, M.; Zhang, J.; Zuo, G.; Lv, X.; Liu, Y.; Shi, C. MCR-ALS-based muscle synergy extraction method combined with LSTM neural network for motion intention detection. *Front. Neurorobot.* **2023**, *17*, 1174710.

Disclaimer/Publisher’s Note: The statements, opinions and data contained in all publications are solely those of the individual author(s) and contributor(s) and not of MDPI and/or the editor(s). MDPI and/or the editor(s) disclaim responsibility for any injury to people or property resulting from any ideas, methods, instructions or products referred to in the content.